Catalysis Today 177 (2011) 55–63

Contents lists available at ScienceDirect

Catalysis Today

journal homepage: www.elsevier.com/locate/cattod

# Theory meets experiment: Electrocatalysis of hydrogen oxidation/evolution at Pd–Au nanostructures

P. Quaino [b,c], E. Santos [a,b,*], H. Wolfschmidt [d], M.A. Montero [d], U. Stimming [d,e]

[a] Facultad de Matemática, Astronomía y Física, Instituto de Física Enrique Gaviola (IFEG-CONICET), Universidad Nacional de Córdoba, 5000 Córdoba, Argentina
[b] Institute of Theoretical Chemistry, Ulm University, D-89069 Ulm, Germany
[c] PRELINE, Fac. Ing. Química, UNL, 3000 Santa Fe, Argentina
[d] Department of Physics E19, Technische Universität München, D-85748 Garching, Germany
[e] ZAE Bayern Division 1, Walther Meißner Strasse 6, D-85748 Garching, Germany

ARTICLE INFO

*Article history:*
Received 7 February 2011
Received in revised form 3 May 2011
Accepted 4 May 2011
Available online 12 July 2011

*Keywords:*
Electrocatalysis
Nanostructures
Electron transfer reactions
d-bands
Hydrogen oxidation/evolution
Pd
Au(1 1 1)

ABSTRACT

The oxidation and evolution reactions of hydrogen are investigated at nanostructures of palladium–gold combining experimental and theoretical approaches. The extraordinary reactivity of submonolayers of Pd on Au(1 1 1) has been explained by a direct correlation with the changes in the electronic properties and geometrical arrangements. The application of the electrocatalysis theory, which goes beyond the qualitative approach of the d band centers, allows explaining quantitatively the experimental finding.


## 1. Introduction

The hydrogen oxidation/evolution reactions (HOR/HER) have been intensively investigated by experimental as well as theoretical research groups. The HER can occur in two different reaction pathways, the Tafel–Volmer [1,2] and the Heyrovsky–Volmer [1,3] pathway. Molecular hydrogen is formed by the recombination of two adsorbed hydrogen atoms in the Tafel–Volmer reaction. The Heyrovsky–Volmer reaction describes the formation of molecular hydrogen from one adsorbed hydrogen atom and one proton from the electrolyte, which is discharged at the adsorbed hydrogen atom on the surface. Therefore the adsorption of atomic hydrogen is the important issue. Moreover, the above described elementary steps are also consequential for the HOR.

Hydrogen reactions have been studied on polycrystalline as well as single crystal noble metal surfaces (see [4–9] and references within). It has been found that the reactivity of different bare surfaces towards hydrogen reactions is strongly influenced by surface orientation. Noble metal catalysts on foreign host supports show surprising findings compared to bare single crystal studies. It has been experimentally shown by several groups [10–19] that the physical and chemical properties of thin Pd overlayers change with respect to the Pd bulk material. Baldauf and Kolb [11] investigated the catalytic behaviour of Pd overlayers on Au(1 1 1) regarding formic acid oxidation. They found that the reactivity is dependent on the thickness of the Pd layer, the crystallographic orientation and also on the chemical identity of the substrate. The oxygen reduction reaction (ORR) has been investigated by Naohara et al. [14,15] on thin Pd layers on Au(1 1 1) and Au(1 0 0). They also found a dependence of the catalytic activity on the thickness of the Pd overlayer. Adsorption and desorption processes of hydrogen have been investigated on Pd overlayers at different single crystal surfaces in the group of Kolb [10,12,13]. Their results show that overlayer thickness as well as the supporting metal influence the adsorption and desorption behaviour and thus the electrocatalytic activity as evidenced by a shift in adsorption potential of hydrogen. Kibler et al. [16,20,12] investigated various parameters influencing the HER which can change the catalytic activity of Pd; They explained most of the observed experimental results such as adsorption, desorption and activity for HER by a lateral strain of thin Pd films on Au(1 1 1) electrodes according to the Nørskov model [21]. Markovic and Ross [22] studied the system Pd on Pt(1 1 1). It has been found

* Corresponding author at: Facultad de Matemática, Astronomía y Física, Instituto de Física Enrique Gaviola (IFEG-CONICET), Universidad Nacional de Córdoba, 5000 Córdoba, Argentina.
*E-mail address:* esantos@uni-ulm.de (E. Santos).

0920-5861/$ – see front matter © 2011 Elsevier B.V. All rights reserved.
doi:10.1016/j.cattod.2011.05.004

that an improvement of the catalytic activity towards the HER and HOR compared to pure Pt(1 1 1) also exists for this system. Experimental results for the hydrogen evolution on Pd decorated vicinal stepped Au single crystal surfaces with various densities of steps have been investigated by Hernandez and Baltruschat [23,24]. Their results indicate the importance of step sites for the electrocatalytic reactivity of Pd-layers. More recently, Pandelov and Stimming [18] reported an increased specific reactivity of Pd submonolayers on Au(1 1 1) which is two orders of magnitude higher compared to bulk Pd when the amount of Pd from multilayers is lowered down to less than 0.05 ML. A spill-over mechanism of the adsorbed hydrogen during the HER from the Pd sites to the Au substrate has been proposed to explain the results for submonolayer coverage [25]. Local reactivity measurements and combined Density Functional Theory (DFT) calculations of Pd and Pt nanoparticles on Au(1 1 1) electrode surfaces have been performed in the group of Stimming [19,26,27]. Experimentally it has been demonstrated by Meier et al. [19] that with decreasing particle size from 200 nm to 6 nm the specific electrochemical activity of single nanoparticles for HER is increased by more than two orders of magnitude. This result has been tentatively explained by a strain effect on the isomorphically deposited Pd particles induced by the Au(1 1 1) substrate with larger lattice constant. However, similar effects have not been found for noble metal particles on HOPG as support material indicating the importance of the support [28]. A possible starting point for fundamental research in electrocatalysis in order to screen substrate effects can be provided by a wide range of combinations of host and solute elements large single crystalline supports suitable for electrochemical environment [29].

Apart from substrate effects, investigations on ultra microelectrodes [30,31] and highly dispersed particles on carbon supports [32,33] also show higher specific activities. It has been shown that higher activity due to enhanced mass transport compared to planar systems should be taken into account.

The experimental results reviewed above have been ascribed to several effects regarding electronic and geometric factors such as a strain effect in the lattice [21,34], high activity of low coordinated atoms [23,24,35], a direct involvement of the gold surface [25] and enhanced mass transport [30–33]. However, a complete understanding that describes the overall effect has not been clearly addressed until now.

The experimental findings have been frequently supported by theoretical work from the groups of Nørskov [34,36,37] and Groß [35,38–40] based on DFT calculations. Nevertheless, some of us have proposed the first theory of electrocatalysis [41–46], which combines elements of the Marcus–Hush theory [47,48] of electron transfer, and the Anderson–Newns model [49,50] for adsorption. DFT calculations are used in our theory as a tool to obtain some of the parameters to be inserted as input in the Santos–Koper–Schmickler (SKS)–Hamiltonian [41,42]. This theory explicitly allows the consideration of solvent and potential effects. Consequently, realistic calculations for an electrochemical environment can be carried out, and the interaction of the orbitals of the reactant and the d band of the electrocatalyst, when either fluctuations of the solvent or the applied potential shift their relative positions, can be understood. Recently, we have applied our theory of electrocatalysis to investigate the reactivity of various nanostructures [51–54]. Particularly, we have given a detailed quantitative analysis of the contribution of different effects, such as strain and chemical interactions on the reactivity of the nanostructures [54]. Thus, the experimental results obtained for monolayers of Pd on different substrates have been explained.

In the present work, we combine experimental as well as theoretical studies to obtain a closer look into the effects of foreign supports on catalytically active noble metals for their activity. The main challenges when theory and experiment meet, is to find a common language connecting the results obtained by means of these two approaches. The accessibility of the systems to be investigated may be different at the atomic level. On the one hand, a wide range of structures and arrangements can theoretically be explored. In many cases, some of them are impossible to obtain experimentally, but the theoretical analysis provides a full picture of the effects that are present in real systems. A nice example of this situation is the calculation of the electronic structures of potentially good catalysts using the lattice constants of other systems. We have applied this strategy in a previous work [54] which has allowed us to separate geometrical from chemical effects on the catalytic properties of monolayers of Pd on different substrates. On the other hand, the dimension of nano-particles employed in real catalysis implies clusters of at least 100–200 atoms, too large for DFT calculations. For this purpose Pd decorated Au(1 1 1) serves as a well investigated model system with well defined parameters and stable experimental conditions. The conclusive results from experiment and theory will be highlighted in the discussion to explain the extraordinary behaviour of submonolayers of Pd on Au(1 1 1).

## 2. Experimental details

Electrochemical Pd deposition on Au(1 1 1) was performed with an EC-Tec BP 600 bipotentiostat/galvanostat and waveform generator (Agilent arbitrary 33220A). Data were recorded with a digital oscilloscope. The electrochemical reactivity measurements with respect to the HOR were done with a potentiostat (HEKA PG 310) using potentiostatic pulses in a standard three-electrode arrangement. A Veeco Multimode EC-SPM/AFM system and a homebuilt Veeco/MI EC-STM system under dry and electrochemical conditions were used for the morphological characterization of the Pd/Au(1 1 1) electrodes. All STM images were taken in constant current mode using etched Au tips or cut Pt/Ir (atomic ratio 80:20) tips. Gold substrates (Schroer GmbH) consisting of 0.7 mm borosilicate glass, 2.5 nm chromium and 250 nm gold layer with a square size of 11 mm × 11 mm) were used as electrodes. Solutions were prepared from $HClO_4$ (Merck, Suprapur), $Pd(NO_3)_2$ (MaTeck, pro analysis) with deionized clean water obtained from a Millipore-Milli-Q (18.2 MΩ/cm, 3 ppm total organic carbon).

The gold substrates were flame annealed and cooled down in Ar atmosphere. This annealing procedure leads to a (1 1 1) orientation of the gold surface. After annealing, the substrates were transferred with a droplet of Milli-Q water to the electrochemical cell in order to avoid contamination. 0.1 M $HClO_4$ solution containing 0.5 mM $Pd(NO_3)_2$ was used for Pd deposition. Pd/Au(1 1 1) was characterized in an Ar-purged 0.1 M $HClO_4$ electrolyte. The pulse deposition procedure starts at an initial potential of 860 mV versus NHE. The potential is then set to the deposition potential of 660 mV versus NHE for various times. The amount of deposited Pd on Au(1 1 1) was determined by integrating the current during the electrochemical deposition, by hydrogen adsorption experiments and by STM images of the substrates, whereas a full monolayer of Pd, deposited from the $Pd^{2+}$-containing solution, corresponds to a charge of 420 $\mu C\,cm^{-2}$. Reactivity measurements of the Pd/Au(1 1 1) system were carried out in $H_2$ purged 0.1 M $HClO_4$.

In the electrochemical STM a gold spiral was used as counter electrode. Prior to measurements the electrode was flame annealed. An oxidized gold wire was used as a reference electrode. The gold wire was cleaned by flame annealing and prepared by anodic oxidation in 0.1 M $HClO_4$ at 12 V for approx. 5 min. Gold tips with Apiozon wax insulation served as probes. The morphology analysis of the STM images such as Pd coverage particle height and total island perimeter length were evaluated with WSxM 4.0 Develop 8.5 (Nanotec Electronica S.L.) [55]. The ratio of particle

**Table 1a**
Adsorption energy for hydrogen on different nanostructures of Pd–Au calculated by DFT. (V) Pure metal surfaces –Pd(1 1 1) and (I) Au(1 1 1)–, two different kind of defect on Au(1 1 1) surface: (II) Au-vacancy and (III) Au-adatom; (VI) a monolayer of Pd on Au(1 1 1), (VII,VIII) $Pd_n$ ($n$ = 3,4) clusters on Au(1 1 1).

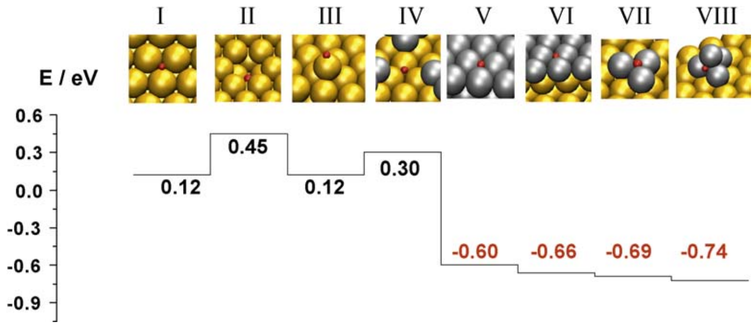


area and total length perimeter and the distance to the first order neighbours was directly calculated via WSxM.

## 3. Computational details

All calculations were performed using the dacapo code [56]. This utilizes an iterative scheme to solve the Kohn–Sham equations of density-functional theory self-consistently. A plane-wave basis set is used to expand the electronic wave functions, and the inner electrons were represented by ultrasoft pseudopotentials [57], which allow the use of a low-energy cutoff for the plane-wave basis set. An energy cutoff 450 eV, dictated by the pseudopotential of each metal, was used in all calculations. The electron–electron exchange and correlation interactions are treated with the generalized gradient approximation in the version of Perdew et al. [58]. The Brillouin-zone integration was performed using a $8 \times 8 \times 1$ $k$-point Monkhorst-Pack grid [59] corresponding to the $1 \times 1$ surface unit cell. Unless mentioned, spin-polarization was not considered. Dipole correction was used to avoid slab–slab interactions [60].

To study the hydrogen adsorption several types of systems were considered: pure metal surfaces –Pd(1 1 1) and Au(1 1 1)–, a monolayer of Pd on Au(1 1 1), $Pd_n$ ($n$ = 3,4) clusters on Au(1 1 1) and finally, two different kind of defects on Au(1 1 1) surface: a Au-vacancy and an Au-adatom.

The pure metal surfaces –Pd(1 1 1) and Au(1 1 1)– were modeled by a $(3 \times 3)$ supercell with 4 metal layers. For the alloy a $(3 \times 3)$ supercell with 4 substrate-layers –Au(1 1 1)– and one adatom-overlayer were used. In the case of the nanostructures, the gold substrate was modeled by a $(3 \times 3)$ supercell with 4 layers. Two nano-arrangements were investigated: a 2D cluster consisting of 3 Pd adatoms and a 3D cluster with 4 Pd adatoms.

In all the calculations 10 layers of vacuum were considered. For all the systems, the two bottom layers were fixed at the next-neighbour distance corresponding to bulk, and all the other layers were allowed to relax. The convergence criterion was achieved when the total forces were less than 0.02 eV/Å.

For the adsorption of H, a single H atom was adsorbed on the adsorption sites and allowed to relax in the $xyz$ coordinates to find the equilibrium position. The effect of the hydrogen coverage was also investigated for the 2D cluster $Pd_3Au$(1 1 1) and the integral adsorption energies were evaluated.

To understand the effects of the coverage and the shape of nanostructures on the hydrogen reaction different coverages and arrangements of Pd atoms on Au(1 1 1) were studied. The selected distributions were: homogenous, rows, and 2D clusters. All these configurations were considered to be deposited on the gold surface or embedded in the surface. The following coverages were checked for all the previous configurations: 0.11, 0.25, 0.33, 0.5, 1.0 and the projected density of states of the d-band for each system has been obtained.

## 4. Results and discussion

### 4.1. Energetic aspect of the hydrogen adsorption

We have systematically analyzed the electronic properties of different nanostructures of Pd–Au and investigated the hydrogen reactions. In the first step, we have calculated by DFT the adsorp-

**Table 1b**
Adsorption of additional hydrogen atoms at the three atom cluster of Pd.

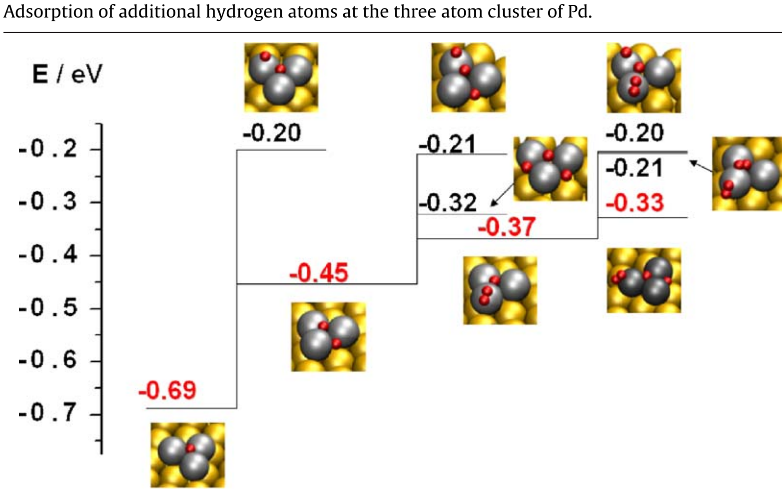

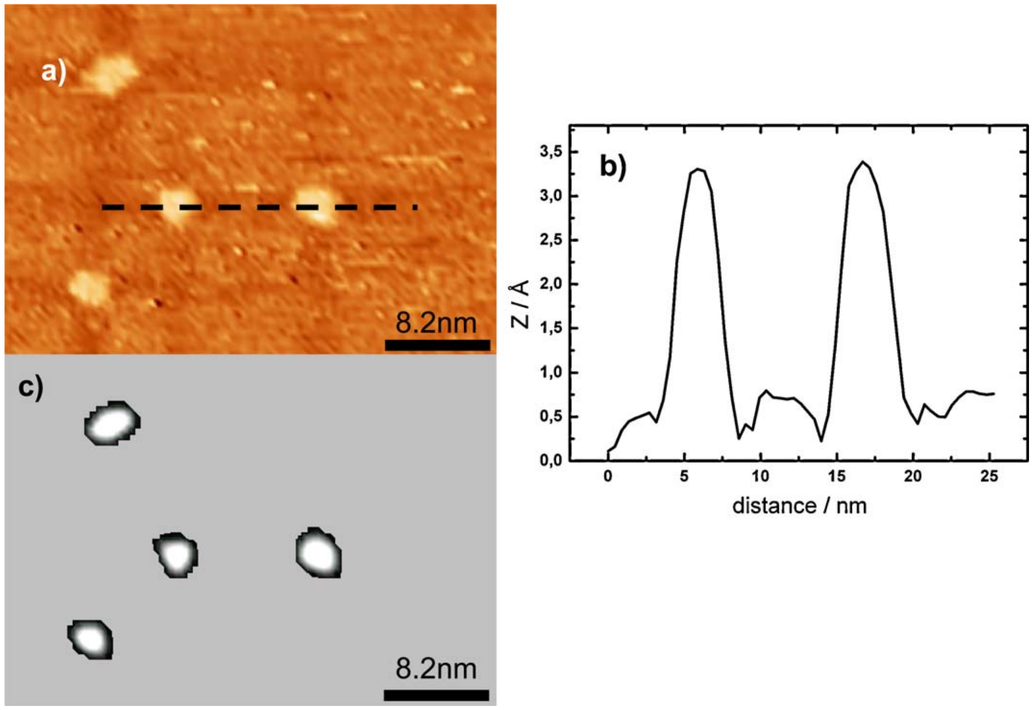


**Fig. 1.** a) STM image of Pd submonolayers on Au(1 1 1), dotted line for cross section. b) Cross section of two particles with one monolayer high Pd. c) Gray scale image of a) in order to obtain surface area and perimeter (indicated in green) for Pd particles. (For interpretation of the references to color in this figure legend, the reader is referred to the web version of the article.)

tion energy of a hydrogen atom at the equilibrium position of the more favorable site of possible structures of Pd–Au. The results are shown in Table 1a). It is clear, that the adsorption of hydrogen on gold requires higher energies than on palladium sites ($E = 0.12$ eV for bare surface). Also for defects, such as gold adatoms ($E = 0.12$ eV like at flat surface) or vacancies ($E = 0.45$ eV) and at gold sites surrounded by palladium atoms ($E = 0.3$ eV) the values are positive. On the contrary, palladium shows a high reactivity ($E = -0.60$ eV for bare surface), specially at nanostructures. Effectively, the calculated adsorption energy of hydrogen at a cluster of four atoms of Pd on Au(1 1 1) is about 0.15 eV more negative than at a flat surface of Pd(1 1 1).

The monolayer of palladium ($E = -0.66$ eV) and the cluster of three palladium atoms ($E = -0.69$ eV) show an intermediate reactivity. Further (see Table 1b)), we have calculated the energy required to adsorb additional hydrogen atoms at different possible sites of the cluster of three Pd atoms on Au(1 1 1) with the first hydrogen at the hollow site. This nanostructure seems to be very reactive for the adsorption of hydrogen. Even the adsorption of four hydrogen atoms at the small cluster gives negative energies with respect to the bare cluster, and it never occurs that hydrogen adsorbs on gold atoms in a stable configuration. There are two possible sites for the adsorption of the second atom at the palladium cluster, on top of a Pd atom and on a bridge position between two palladium atoms. The latter configuration is more favorable ($E = -0.45$ eV), and due to the repulsion between the hydrogen atoms, the second hydrogen is slightly shifted to the surface of gold remaining at a mixture hollow site formed by two palladium and one gold atoms.

The third hydrogen atom prefers the second Pd–Pd–Au-hollow site ($E = -0.32$ eV) instead of the top site on Pd ($E = -0.21$ eV). However, the configuration with the lowest energy ($E = -0.37$ eV) results if the third hydrogen atom approaches the other nonequivalent top site position near the second hydrogen atom. In this case these both atoms strongly interact and come close to each other at a distance near the bondlength of a hydrogen molecule (0.84 Å in comparison, $d_{H_2} = 0.765$ Å). It is noticeable, that this "pre"-molecular state is only formed with the hydrogen adsorbed at the mixture hollow site and not with those at the pure palladium hollow site. Thus, it is expected that the recombination or the Heyrovsky step in the HER at these nanostructures to occur faster than at pure palladium surfaces. Because the adsorption at the mixture hollow site is weaker than at the pure Pd hollow site, it is easier to form the hydrogen molecule by the reaction of this adsorbed atom.

The fourth hydrogen atom prefers a mixture hollow site ($E = -0.33$ eV) to a top site ($E = -0.20$ eV). Nevertheless, the formation of a second "pre"-molecule is also possible if the fourth hydrogen approaches to the top site near the first hydrogen pair ($E = -0.21$ eV).

The very large range of energies obtained by the adsorption of hydrogen on different possible sites of these nanostructures demonstrates the complexity of the system in comparison to flat, homogeneous surfaces.

### 4.2. Structural characterization of the nanostructures

In spite of the incredible technological advances, it is not easy to obtain and to characterize atomic arrangements with the precision that the theoretical studies suggest.

In order to investigate the influence of particle size, particle distance and particle morphology STM was used to obtain a detailed view of the Pd/Au(1 1 1) nanostructured electrodes. It is a challenging task to observe cluster composed of few atoms. One typical example of Pd nanoislands obtained on Au(1 1 1) at room temperature is shown in Fig. 1a). The background shows an atomically flat Au(1 1 1) surface covered by four islands of Pd with a height corresponding to the dimension of atomic Pd. The horizontal dashed line through the two middle particles is plotted as cross section in Fig. 1b). Two uniform particles with similar diameter (approximately 4 nm and 5 nm), an inter-particle distance of 7 nm and the same monoatomic height referred to the ordinate baseline of 0.5 nm, are shown. This result underlines the equal size distribution of electrochemical deposition via potentiostatic pulses for the

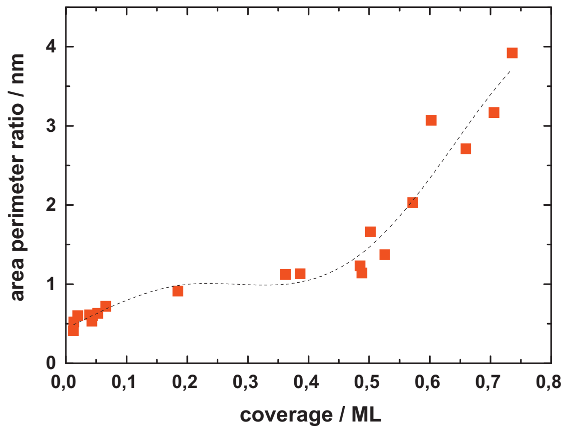


**Fig. 2.** Ratio of area divided by perimeter vs. coverage of Pd in monolayer. (The line is a help to the eye.)

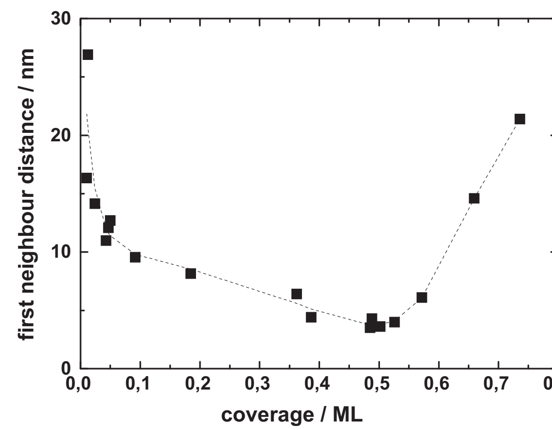


**Fig. 3.** Distance to the first neighbour vs. coverage of Pd in monolayer. (The line is a help to the eye.)

system Pd/Au(1 1 1) for small coverage without any agglomeration. The perimeter and the area of each single particle have been determined with WSxM software and are shown for the four particles. A background correction has been done by flooding the Au(1 1 1) surface shown in Fig. 1c). The Pd coverage on Au(1 1 1) is 2.8%. Particles stay as islands due to higher contrast, which is illustrated in gray scale. The area as well as the perimeter can be determined and evaluated to obtain the total perimeter length, the area of each single particle, the total coverage and the first neighbour distance of Pd on Au(1 1 1).

Fig. 2 shows the area perimeter ratio versus the coverage of Pd on Au(1 1 1). It can be clearly seen that the increasing coverage leads to an increasing ratio of the particle area divided by the perimeter. Whereas an increase of about one order of magnitude in the whole range is seen, there are three major parts. Below 0.1 ML the ratio increases by more than a factor of two. Between 0.1 ML and 0.5 ML the ratio is only slightly increasing followed by an increase of more than a factor of three for coverage higher than 0.5 ML. Especially in the range for more than a half monolayer the nanoislands grow together which strongly influences the ratio of area to perimeter. Interestingly there is also a strong effect below 0.1 ML where a large change in the ratio is seen when only varying the coverage by a few percent indicating a strong decrease for smaller particles with a strong variation in the ratio of terrace atoms and edge atoms.

In order to investigate the distribution of nanoparticles prepared by random electrochemical deposition methods using potentiostatic pulses an additional evaluation has been performed to obtain a parameter for structural analysis. As an average value for the Pd/Au(1 1 1) electrode for particle separation the first neighbour distance can be determined. This allows a rough estimation of the inter particle distance although the particle distribution is not perfectly uniform across the surface. As it can be seen in Fig. 3 the first neighbour distance increases with decreasing coverage for smaller than 0.5 ML. A large separation for smaller particles especially with a strong increase in the range smaller than 0.1 ML is obvious. The coalescence together for larger coverage and thus less single separated particles results also in an increasing first neighbour distance for coverage larger than 0.5 ML.

In spite of the high accuracy of these experiments, the size of the islands characterized by STM is much larger than the clusters used for the theoretical calculations. However, when the coverage decreases, in the real system the number of sites such as those of the few atoms clusters described above, also increases. Because of their high activity, they mainly determine the catalytic activity. Also, it is possible that such small clusters are present at the surface, but the size is below the detection level of the STM measurements.

### 4.3. Electronic analysis of the nanostructures

Fig. 4 shows the electronic density of states for the d and sp bands of different systems with flat surfaces. The bands of the Pd(1 1 1) surface extend just up to the Fermi level, while those of Au(1 1 1) surface are negatively shifted about of 1.5 eV. Only this distinction makes palladium a better catalyst than gold and a qualitative description based on the position of the band center is sufficient ($\varepsilon_c^d = -1.82$ eV and $\varepsilon_c^d = -3.5$ eV for Pd and Au respectively). For mixed systems the situation is more complicated. There are strain effects, but also the chemical interactions between the substrate and the adlayer play a very important role, as can been observed by comparing Fig. 4c) and d). The analysis of a virtual system calculated using the lattice constant of Au(1 1 1) for a Pd(1 1 1) surface allows to separate these two effects. In this case only the strain effect is present, and it produces sharper bands due to the higher localization, but the distribution of electronic states is similar (see Fig. 4c)) and compare red and orange curves). In the case of a monolayer of Pd on Au(1 1 1) surface, both effects are present and thus the distribution of electronic states changes in comparison to bare surface of Pd(1 1 1) (see Fig. 4d)). Effectively, the d band of palladium is sharper and the peak at −0.5 eV is particularly high. Also, the sp band of palladium shows important changes with a complicated structure, which reveals the bonding with the gold surface. In fact, the sp band of palladium now shows electronic states in the region from −9 to −5 eV, indicating an overlap with the sp band of the gold substrate.

The behaviour of submonolayers of palladium on gold strongly depends on the geometrical arrangement of the nanostructures. The electronic density of states is different for different distributions of the palladium atoms. Fig. 5 shows the calculated density of states at a constant composition of 0.33 Pd atoms, but with different configurations. Also the same distribution of atoms has different electronic properties if the nanostructure is embedded in the surface of gold or adsorbed above the surface. As expected, the structures with lower coordination give the sharper peaks because of the larger electronic localization. In addition, the interaction of the sp bands of gold and palladium is evident from Fig. 5. In the case of the adsorbed nanostructures, like the monolayer (see Fig. 4d)), the contribution of gold and palladium to the overlap can be clearly distinguished. The embedded structures show a larger mixture of these states and the lower edge of the sp band extends up to intermediate energies between the values of gold and palladium. These results are a clear evidence that an interpretation of the catalytic activity of these systems based only on the position of the d-band centers and strain effects is insufficient.

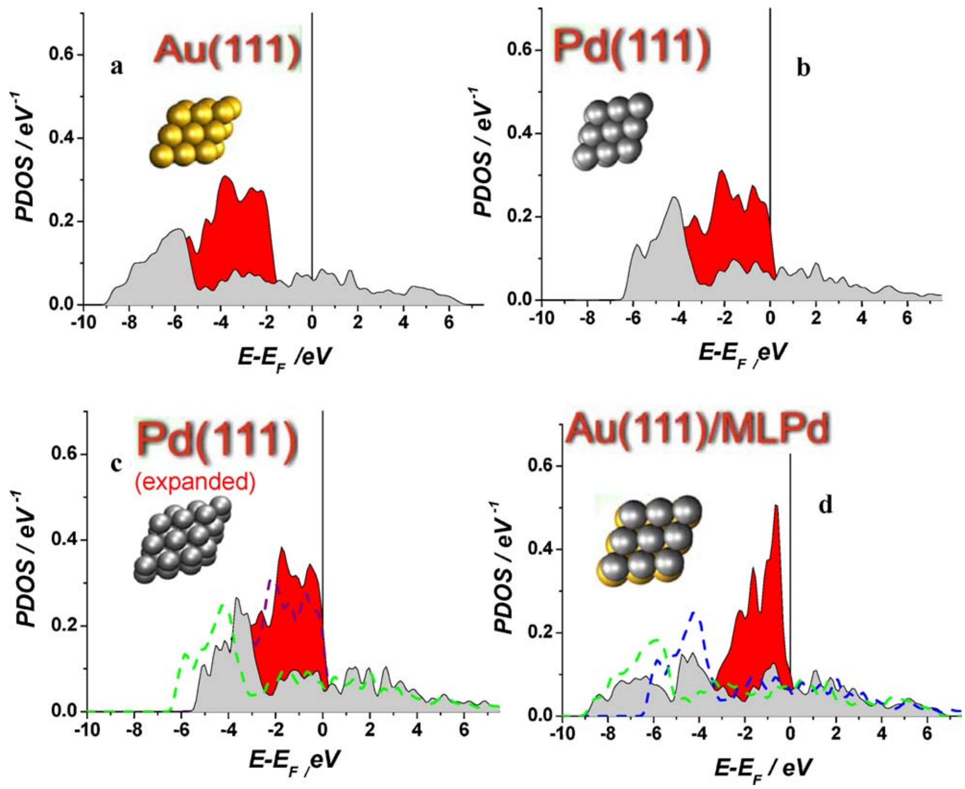


**Fig. 4.** Electronic density of states projected onto the d-band (red shaded area) and onto the sp-band (gray shaded area) for different systems. a) flat surface of Au(1 1 1); b) flat surface of Pd(1 1 1); c) virtual expanded flat surface of Pd(1 1 1) calculated with the lattice constant of Au; sp-band for the not expanded surface (green dashed line); d-band for the not expanded surface (purple dashed line) d) commensurate monolayer of Pd on Au(1 1 1); sp-band of bare Au(1 1 1) (green dashed line); sp-band of bare Pd(1 1 1) (blue dashed line). The vertical line indicates the position of the Fermi level. (For interpretation of the references to color in this figure legend, the reader is referred to the web version of the article.)

Fig. 6 shows the effect on the electronic properties of the system due to the interaction of the nanostructures with a hydrogen atom approaching to the surface of a three palladium cluster on Au(1 1 1). Similar features have been observed with other nanostructures. In the past, when the reactivity of a catalyst has been investigated, the attention has been exclusively focused to the d-bands. The sp bands have been underestimated because it was thought they are wide, structureless and similar for all the metal-

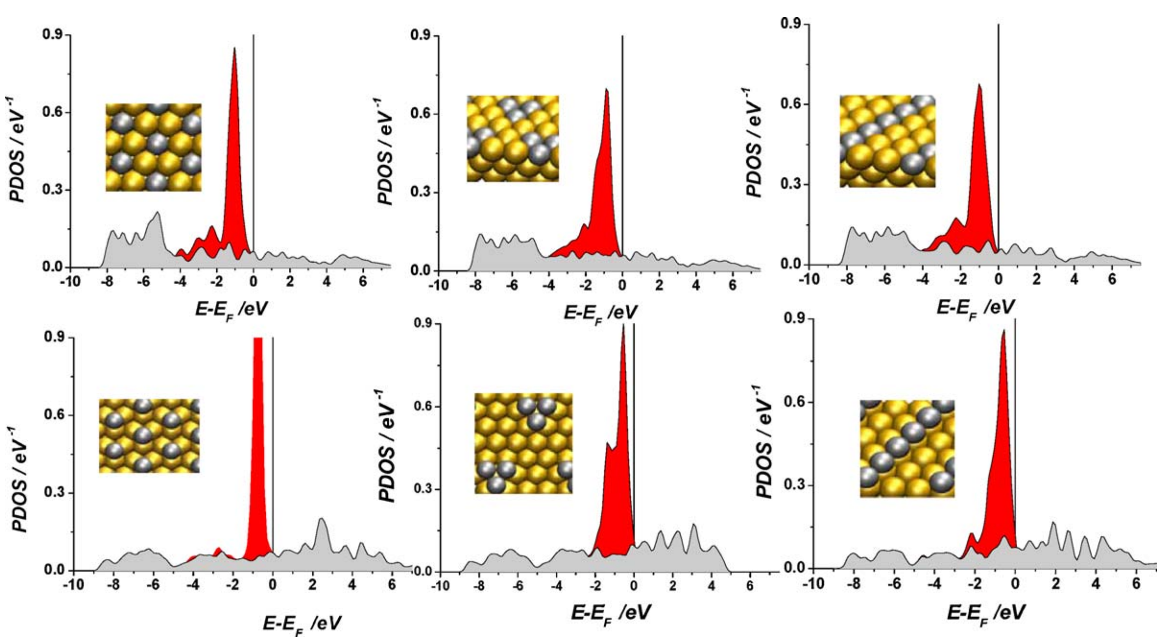


**Fig. 5.** Electronic density of states at constant composition (0.33 Pd) projected onto the d-band (red shaded area) and onto the sp-band (gray shaded area) of palladium for different atomic arrangements; embedded atoms (top, a)–c)) and adatoms (bottom, d)–f)); homogeneous distribution (a)–d)); three atoms clusters (b)–e)); row distribution (c)–f)). The vertical line indicates the position of the Fermi level. (For interpretation of the references to color in this figure legend, the reader is referred to the web version of the article.)

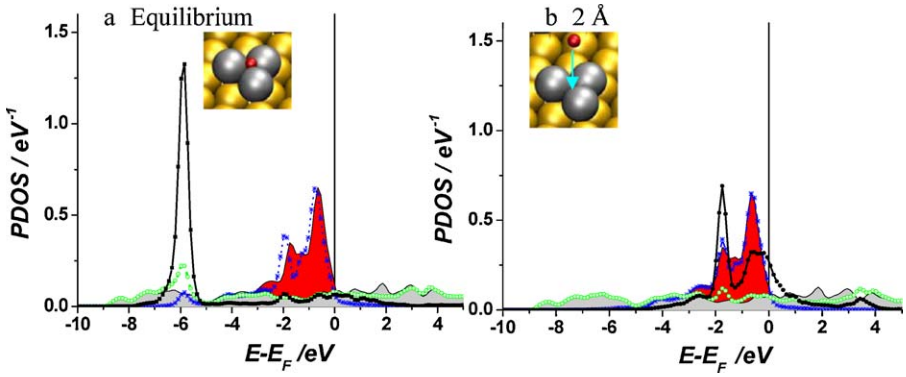


**Fig. 6.** Electronic density of states when a hydrogen atom approaches a three palladium cluster on Au(1 1 1). a) Hydrogen adsorbed at the cluster at the equilibrium position. b) Hydrogen at a distance of 2 Å from the equilibrium position. The states are projected: onto the d-band of palladium (blue line with stars), onto the sp of palladium (green line with open circles) onto the s orbital of hydrogen (black line with full squares). The d band (red shaded area) and the sp-band (gray shaded area) of palladium in the absence of hydrogen are also shown. The vertical line indicates the position of the Fermi level. (For interpretation of the references to color in this figure legend, the reader is referred to the web version of the article.)

lic systems. Although it is true that the electronic states of the d bands play a key role in the catalysis when the hydrogen 1s orbital is passing the Fermi level, the interaction with the sp bands is also important in the formation of the bond to the surface at the final state of the reaction. It is clear from Fig. 6 that the 1s orbital of hydrogen interacts with both bands in a concerted way. The electronic distribution of both bands is modified in the presence of hydrogen. An overlap of peaks corresponding to bonding states between the 1s orbital, sp and d bands is observed at about −5.8 eV when hydrogen is adsorbed at the equilibrium position (see Fig. 6a)). In the region where the d band appears, the 1s orbital shows a broad distribution. However, a small peak at about −2.0 eV is observed. At these energies the d band also shows a shift of the electronic states resulting in a coincident sharp peak with the 1s orbital. All these bonding states are occupied and consequently they stabilize the adsorbed species. At energies above the Fermi level (≈1.8 eV) a slight depletion of the sp band is observed, which compensates the excess produced by the peak at −5.8 eV. The 1s orbital slightly extends above the Fermi level. These observations seem to indicate a partial transfer of electrons from the hydrogen to the metal. However, because the sp band extends up to large distances of the surface, it does not mean that a polarization of the metal–hydrogen bond appears. Thus, there are no contradictions with the experimental facts that hydrogen covalently binds to the metal.

At larger distances of the hydrogen atom (2 Å), this complicated interplay of interactions is also evident. At −1.75 eV three coincident peaks of the 1s orbital, sp and d bands appear. At about 3 eV above the Fermi level, an overlap of unoccupied anti-bonding states between the sp band and the 1s orbital can be observed.

Fig. 7 shows the electronic structure of a homogeneous distribution of different amounts of palladium for embedded systems (Fig. 7a)) and adatoms (Fig. 7b)). Very sharp d bands are observed due to the localization. This effect increases at lower amounts of Pd since the separation between the atoms also increases. The adatoms show the larger localization, as expected. It is interesting to note, that for the latter, up to a composition of 0.33 no changes are observed for lower ratios of Pd. It indicates that at the lower content of Pd the distances are so large, that no more interactions between the Pd atoms takes places. It is not the case for the embedded atoms, where they are interacting through the gold atoms bonded to them.

### 4.4. Effect of the composition of Pd–Au nanostructures on the hydrogen oxidation and evolution reactions

Pd modified Au(1 1 1) surfaces have been investigated in $H_2$ saturated 0.1 M $HClO_4$ using potentiostatic pulses at various overpotentials. The current transients for the HOR were evaluated using $j$ versus $t^{1/2}$ plot in order to separate the kinetic current from the mass transport limiting current [17,61]. Kinetic current transients for the overpotentials +100 mV, +200 mV and +300 mV with respect to the hydrogen oxidation were evaluated. Fig. 8 shows the kinetic currents versus the Pd coverage on the Au(1 1 1) surfaces in the upper part in the range lower than one complete monolayer. The determination of the active material assumes that only Pd is active in the reaction and Au(1 1 1) acts as inactive support. The specific current with respect to the Pd area on the Au(1 1 1) surface increases with decreasing amount of Pd for less than one ML by more than one order of magnitude for 0.1 ML of Pd. The data indicate a strong increase in specific reactivity of Pd with decreasing

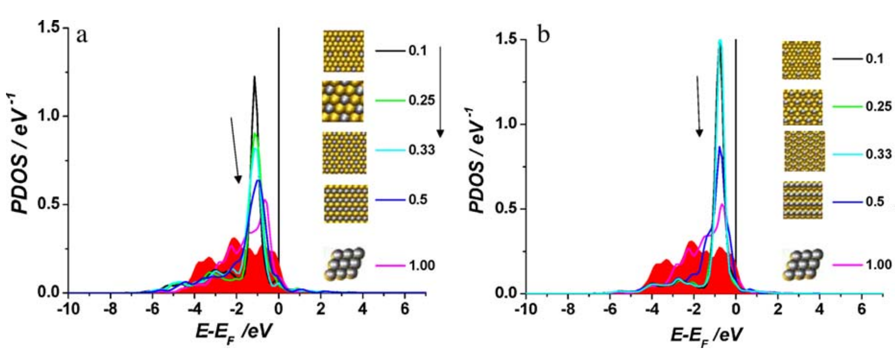


**Fig. 7.** Effect on the d band of palladium of different composition of palladium homogeneously distributed on Au(1 1 1). a) Embedded palladium in the gold surface. b) Adsorbed on the gold surface. The d band (red shaded area) of Pd(1 1 1) surface is also shown. The vertical line indicates the position of the Fermi level. (For interpretation of the references to color in this figure legend, the reader is referred to the web version of the article.)

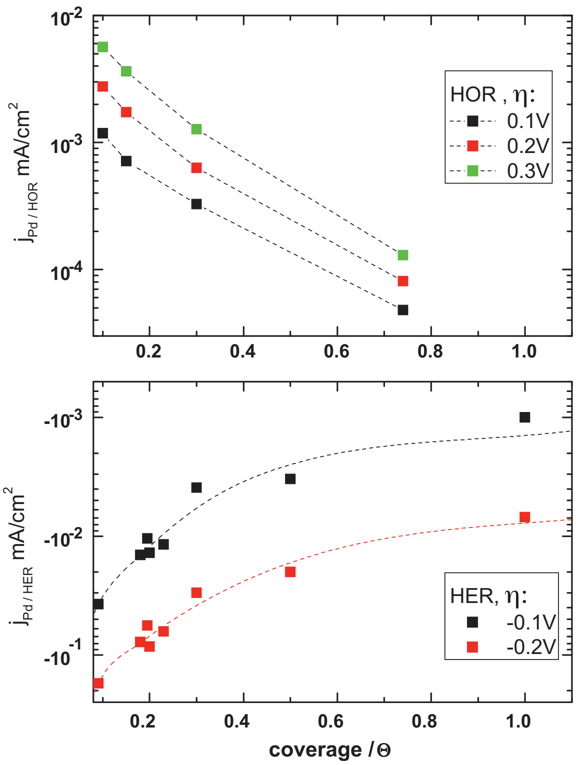


**Fig. 8.** Specific current density for Pd on Au(1 1 1) vs. Pd coverage for the HOR and HER at different overpotentials.

amount of Pd from 0.74 ML to 0.1 ML. Hence, current densities of close to 8 mA/cm$^2$ per Pd area at +300 mV are observed.

The results on HER were extracted from [18]. As compared to the results for the HOR a similar increase in reactivity for decreasing amount of noble metal can be observed. Although the net currents are higher as compared to the HOR the increase is also in the range of more than one order of magnitude in the range between one full monolayer and 0.1 ML. The difference in the absolute values can be attributed to an influence of diffusion limitation of hydrogen molecules in the case of HOR although the potential pulse technique and the evaluation procedure try to avoid this.

Further, we have applied our theory of electrocatalysis to calculate the exchange current density for the oxidation reaction of hydrogen at the different composition of palladium in the gold surface. We have used a similar procedure as in [53] and used the SKS-Hamiltonian to obtain the potential energy surface as a function of the solvent coordinate $q$ and the separation distance between two atoms of hydrogen for the global reaction:

$$H_2 \rightarrow 2H^+ + 2e^-$$

The details of the theory are given in previous publications [42,44,53]; here, we summarize those aspects which are essential for understanding the application to hydrogen oxidation. Explicitly, we consider the reaction of a biatomic homonuclear molecule at a metal electrode. The Hamiltonian of the system contains the contributions of the molecule, the metal which acts as a catalyst, the solvent and the corresponding interactions between these subsystems. In order to describe the molecular bond between the two hydrogen atoms, we employ the extended Hückel approximation taking into account the repulsion by orbital overlap. The Marcus–Hush theory [47,48] is applied for the reorganization of the solvent and the Anderson–Newns model [49,50] for the interaction of the valence orbital with the metal. Other interactions, such as spin–spin repulsion on the reactant and image charge, are

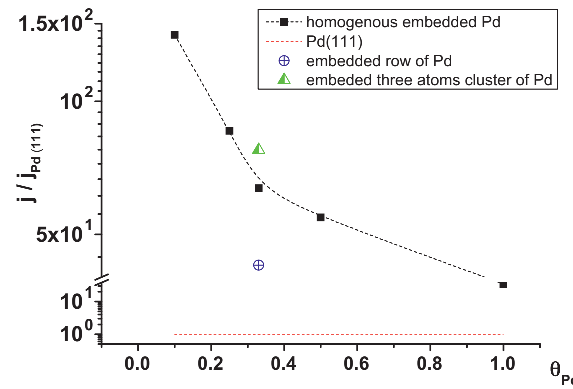


**Fig. 9.** Theoretical values of the exchange current for the HOR normalized to the surface of Pd(1 1 1) for different composition of palladium embedded in a surface of Au(1 1 1) calculated with the electrocatalysis theory and the electronic structures of Fig. 8a). For comparison, the values obtained with a embedded row and a embedded three Pd atoms clusters in the Au(1 1 1) are included. The dotted red line indicates the value of 1 for the Pd(1 1 1) surface. Parameter used for the calculation: $U$ = 4.54 eV; $\lambda$ = 2.0 eV; $|V_d|^2$ = 6.3 eV$^2$; $|V_{sp}|^2$ = 1.0 eV$^2$; $\beta_o$ = −4.55 eV. (For interpretation of the references to color in this figure legend, the reader is referred to the web version of the article.)

also considered. Then, the Hamiltonian is solved within the Green's functions formalism. For a homonuclear molecule, the density of states of the reactant is affected by the presence of the metal and can be described by the following expression:

$$\rho_{\text{Molec}} = \frac{1}{\pi}\sum_{\sigma}\left\{\frac{\Delta}{\left(z-\tilde{\varepsilon}_{\sigma}-\beta\right)^{2}+\Delta^{2}}+\frac{\Delta}{\left(z-\tilde{\varepsilon}_{\sigma}+\beta\right)^{2}+\Delta^{2}}\right\} \quad (1)$$

The sum is over the two spin states $\sigma = \pm 1$; the first term corresponds to the bonding and the second one to the anti-bonding orbital. The parameter $\beta$ is related to the dissociation energy of the molecule $D_e$ and thus determines the energy separation between both orbitals. The effective energy of the orbital of one constituent atom is given by $\tilde{\varepsilon}_{\sigma}$:

$$\tilde{\varepsilon}_{\sigma\pm} = \varepsilon^{o} + S\beta - 2\lambda\hat{q} + U\langle n_{\sigma\mp}\rangle - \gamma\left(1 - \langle n_{\sigma-}\rangle - \langle n_{\sigma+}\rangle\right) + \Lambda \quad (2)$$

Here $\varepsilon^{o}$ is the energy of the atomic orbital relative to the Fermi level; it can be tuned by the applied electrode potential. The second term accounts for the orbital overlap $S$ between both atoms. The third term is the shift produced by the fluctuations of the solvent, where $\lambda$ is the reorganization energy according to Marcus–Hush theory, and $q$ the normalized solvent coordinate. The fourth and fifth terms account for the spin–spin and dipole–dipole interactions respectively. $\langle n_i\rangle$ is the occupation of the spin orbital $i$. $\Delta$ and $\Lambda$ are the so called chemisorption functions, which are related to the density of states of the metal and the coupling constant between metal and molecule $V_k$.

Fig. 9 shows the normalized exchange currents of the hydrogen oxidation obtained from our theory for a series of different composition of Pd embedded in the surface of Au(1 1 1). Comparing these results with the experimental data of Fig. 8 for the measured currents we can conclude that our theory applies well to these systems. Effectively, both experimental and theoretical values increase by about an order of magnitude when the coverage of Pd decreases, indicating an appreciable diminishing of the activation barrier for the processes implied in the reaction. Also it is interesting to note, that although the center of the d bands for the three atoms cluster, for the row and for the homogeneous distribution is almost the same ($\varepsilon_c^d = -1.6$ eV), the electrocatalytic activity is different (see Fig. 9). This is a clear demonstration of the limit of applying the d band center theory. This can explain qualitatively some tendencies, but to obtain quantitative results the whole distribution of electronic states must be considered.

## 5. Conclusions

Dealing with nanomaterials is a challenge for both, experiments and theory. Hence, our goal was to combine both approaches to elucidate and predict their catalytic activity. In this context, Pd submonolayers on Au substrates have been investigated. The studies have been focused on the HOR and HER. The experimental results have shown that the activity of Au substrates covered by Pd considerably increases when the Pd coverage decreases and small islands with monoatomic height dimension are distributed at the surface. A strong dependence on the atomic arrangements and the amount of palladium has been found. The application of the electrocatalysis theory, which goes beyond the qualitative approach of the d band centers and strain effects, allows explaining quantitatively the experimental finding. A direct correlation with the change in the electronic properties and the electrocatalytic activity has been obtained. The largest effect occurs for the clusters. Here the DOS is strongly shifted towards the Fermi level, with a pronounced peak lying just below the Fermi level. On the monolayer, the DOS is also strongly shifted towards the Fermi level, but the effect is not quite as large as for the clusters. Hydrogen adsorbs preferentially on palladium sites, with the exception at higher coverage, of a mixture hollow site of two palladium atoms and a gold atom at the edge of clusters. This fact plays an important role to decrease the activation barrier for the recombination and Heyrowsky steps. Thus, the reaction at small cluster occurs faster than at large Pd domains, in excellent accordance with the experiments. Effectively, the comparison of experimental and calculated exchange currents for the HER/HOR when the coverage of Pd decreases, shows the same trend.

## Acknowledgements

This work is part of the research network financed by the Deutsche Forschungsgemeinschaft FOR1376. The content has been presented and discussed in the internal meeting of ELCAT and COST (Networks of the European Union). P.Q. acknowledges financial support by PICT-2008-0737 (ANPCyT). E.S. acknowledges financial support by PIP-CONICET 112-201001-00411. E.S. and P.Q. thanks CONICET (Argentina) for continued support. Finally, fruitfully discussions with Prof. W. Schmickler are gratefully acknowledged.

## References

[1] T. Erdey-Gruz, M. Volmer, Z. Phys. Chem. 150 (1930) 203.
[2] J. Tafel, Z. Phys. Chem. 50 (1905) 641.
[3] J. Heyrovsky, Recueil Des. Travaux Chimiques Des Pays-Bas 46 (1927) 582.
[4] N.M. Markovic, B.N. Grgur, P.N. Ross, J. Phys. Chem. B 101 (1997) 5405.
[5] N.M. Markovic, S.T. Sarraf, H.A. Gasteiger, P.N. Ross, J. Chem. Soc. Faraday Trans. 92 (1996) 3719.
[6] J.H. Barber, B.E. Conway, J. Electroanal. Chem. 461 (1999) 80.
[7] J. Barber, S. Morin, B.E. Conway, J. Electroanal. Chem. 446 (1998) 125.
[8] J. Perez, E.R. Gonzalez, H.M. Villullas, J. Phys. Chem. B 102 (1998) 10931.
[9] H. Wolfschmidt, O. Paschos, U. Stimming, in: A. Wieckowski, J.K. Norskov (Eds.), Fuel Cell Science: Theory, Fundamentals, and Biocatalysis, John Wiley & Sons, New York, 2010.
[10] M. Baldauf, D.M. Kolb, Electrochim. Acta 38 (1993) 2145.
[11] M. Baldauf, D.M. Kolb, J. Phys. Chem. 100 (1996) 11375.
[12] L.A. Kibler, A.M. El-Aziz, D.M. Kolb, J. Mol. Catal. A: Chem. 199 (2003) 57.
[13] L.A. Kibler, A.M. El-Aziz, R. Hoyer, D.M. Kolb (Eds.), Angew. Chem. Int. 44 (2005) 2080.
[14] H. Naohara, S. Ye, K. Uosaki, J. Electroanal. Chem. 500 (2001) 435.
[15] H. Naohara, S. Ye, K. Uosaki, Electrochim. Acta 45 (2000) 3305.
[16] L.A. Kibler, Chemphyschem 7 (2006) 985.
[17] H. Wolfschmidt, R. Bußar, U. Stimming, J. Phys.: Condens. Matter 20 (2008) 374127.
[18] S. Pandelov, U. Stimming, Electrochim. Acta 52 (2007) 5548.
[19] J. Meier, J. Schiotz, P. Liu, J.K. Nørskov, U. Stimming, Chem. Phys. Lett. 390 (2004) 440.
[20] L.A. Kibler, A.M. El-Aziz, R. Hoyer, D.M. Kolb, Angew. Chem. Int. Ed. 44 (2005) 2080.
[21] B. Hammer, J.K. Nørskov, Adv. Catal. 45 (2000) 71.
[22] N.M. Markovic, P.N. Ross, Surf. Sci. Rep. 45 (2002) 121.
[23] F. Hernandez, H. Baltruschat, J. Solid. State Chem. 11 (2007) 877.
[24] F. Hernandez, H. Baltruschat, Langmuir 22 (2006) 4877.
[25] M. Eikerling, J. Meier, U. Stimming, Z. Phys. Chem. (Int. Ed.) 217 (2003) 395.
[26] J. Meier, K.A. Friedrich, U. Stimming, Faraday Discuss. 121 (2002) 365.
[27] H. Wolfschmidt, D. Weingarth, U. Stimming, Chemphyschem 11 (2010) 1533.
[28] T. Brülle, U. Stimming, J. Electroanal. Chem. 636 (2009) 10.
[29] H. Wolfschmidt, C. Baier, S. Gsell, M. Fischer, M. Schreck, U. Stimming, Materials 3 (2010) 4196.
[30] S.L. Chen, A. Kucernak, J. Phys. Chem. B 108 (2004) 13984.
[31] P.M. Quaino, J.L. Fernandez, M.R.G. de Chialvo, A.C. Chialvo, J. Mol. Catal. A: Chem. 252 (2006) 156.
[32] H.A. Gasteiger, J.E. Panels, S.G. Yan, J. Power Sources 127 (2004) 162.
[33] K.C. Neyerlin, W.B. Gu, J. Jorne, H.A. Gasteiger, J. Electrochem. Soc. 154 (2007) B631.
[34] M. Mavrikakis, B. Hammer, J.K. Nørskov, Phys. Rev. Lett. 81 (1998) 2819.
[35] A. Gross, Top. Catal. 37 (2006) 29.
[36] B. Hammer, J.K. Nørskov, Surf. Sci. 343 (1995) 211.
[37] A. Ruban, B. Hammer, P. Stoltze, H.L. Skriver, J.K. Nørskov, J. Mol. Catal. A: Chem. 115 (1997) 421.
[38] A. Roudgar, A. Gross, Phys. Rev. B 67 (2003) 033409.
[39] A. Roudgar, A. Gross, J. Electroanal. Chem. 548 (2003) 121.
[40] A. Roudgar, A. Gross, Surf. Sci. 597 (2005) 42.
[41] E. Santos, M. Koper, W. Schmickler, Chem. Phys. Lett. 419 (2006) 421.
[42] E. Santos, M.T.M. Koper, W. Schmickler, Chem. Phys. 344 (2008) 195.
[43] E. Santos, W. Schmickler, Chemphyschem 7 (2006) 2282.
[44] E. Santos, W. Schmickler, Chem. Phys. 332 (2007) 39.
[45] E. Santos, K. Potting, W. Schmickler, Faraday Discuss. 140 (2008) 209.
[46] E. Santos, A. Lundin, K. Potting, P. Quaino, W. Schmickler, Phys. Rev. B 79 (2009).
[47] R.A. Marcus, J. Chem. Phys. 24 (1965) 966.
[48] N.S. Hush, J. Chem. Phys 28 (1958) 962.
[49] P.W. Anderson, Phys. Rev. 124 (1961) 41.
[50] D.M. Newns, Phys. Rev. 178 (1969) 1123.
[51] E. Santos, P. Quaino, G. Soldano, W. Schmickler, J. Chem. Sci. 121 (2009) 575.
[52] E. Santos, A. Lundin, K. Potting, P. Quaino, W. Schmickler, J. Solid State Electrochem. 13 (2009) 1101.
[53] E. Santos, W. Schmickler, Electrochim. Acta 53 (2008) 6149.
[54] E. Santos, P. Quaino, W. Schmickler, Electrochim. Acta 55 (2010) 4346.
[55] I. Horcas, R. Fernandez, J.M. Gomez-Rodriguez, J. Colchero, J. Gomez-Herrero, A.M. Baro, Rev. Sci. Instrum. 78 (2007) 013705.
[56] B. Hammer, L.B. Hansen, J.K. Norskov, Phys. Rev. Lett. 59 (1996) 7413, http://www.fysik.dtu.dk/campos.
[57] D. Vanderbilt, Phys. Rev. B 41 (1990) 7892.
[58] J.P. Perdew, K. Burke, M. Ernzerhof, Phys. Rev. Lett. 77 (1996) 3865.
[59] H.J. Monkhorst, J.D. Pack, Phys. Rev. B 13 (1976) 5188.
[60] L. Bengtsson, Phys. Rev. B 59 (1999) 12301.
[61] W. Schmickler, E. Santos, Interfacial Electrochemistry, Springer, Berlin, 2010.